JOURNAL OF GEOPHYSICAL RESEARCH, VOL. 95, NO. D2, PAGES 1955–1963, FEBRUARY 20, 1990

A Low-Order Dynamical Model of Global Climatic Variability Over the Full Pleistocene

KIRK A. MAASCH AND BARRY SALTZMAN

Department of Geology and Geophysics, Yale University, New Haven, Connecticut

A previously formulated dynamical model of the late Pleistocene ice ages (based on the hypothesis that the global CO_2 system can provide the instability to drive a natural oscillation involving feedbacks between the cryosphere, atmosphere, and ocean) is extended to include (1) additive earth orbital forcing (summer insolation changes at 65°N) and (2) tectonic forcing in the form of a postulated variation in the multiplicative parameters (rate constants) of the model system. The structural (e.g., bifurcation) properties of the model are examined in detail to reveal the regions of parameter space wherein the geologically inferred features of the full Pleistocene can be simulated, including the observed chronology, the phase relationships between ice, CO_2, and North Atlantic Deep Water formation, and the mid-Pleistocene transition.

INTRODUCTION

In a recent paper [*Saltzman and Maasch*, 1988] we described a model for the late Pleistocene ice ages that had a free oscillatory solution driven by instability of the global carbon dioxide system, of a period near 100 kyr, which is the dominant period observed. We now seek to demonstrate that this same model can be extended to account for the main features and the chronology of the full Pleistocene, including the rapid transition near 900 ka [*Pisias and Moore*, 1981; *Start and Prell*, 1984; *Maasch*, 1988] as well as the shorter periods near 20 and 40 kyr that appear to be driven by Milankovitch forcing.

A bifurcation to the dominant 100-kyr period as a free solution can occur in accordance with one of at least two scenarios shown schematically in Figure 1. The first of these, labeled *a*, portrays the early Pleistocene as a steady state which subsequently undergoes a transition into a free oscillation having an approximately 100 kyr periodicity during the late Pleistocene. The second, labeled *b*, has free oscillatory behavior in both the early and late Pleistocene with the early Pleistocene solution oscillating about a mean value which is less than the late Pleistocene mean and having a shorter period than that of the late Pleistocene. Although in these idealized pictures the oscillations are drawn with constant amplitude and period, it is possible that they may actually be either damping or growing with time; growth during the early Pleistocene would be the case discussed by *Saltzman and Sutera* [1987]. Before discussing these possibilities in more detail, we will first review the model briefly along with an example of an improved late Pleistocene solution which includes both asymmetry and external earth orbital forcing.

THE MODEL

The equations developed by *Saltzman and Maasch* [1988] were hypothesized to govern the long-term variations of global ice mass (I), atmospheric CO_2 (μ), and deep ocean warmth and salinity associated, for example, with North Atlantic Deep Water, or NADW (N), and are of the form

$$\dot{I}' = -a_0 I' - a_1 \mu' - a_2 M(t) \tag{1}$$

$$\dot{\mu}' = b_1 \mu' - (b_2 - b_3 N')N' - b_4 N'^2 \mu' \tag{2}$$

$$\dot{N}' = -c_0 I' - c_2 N' \tag{3}$$

where the primes denote departures from an equilibrium state controlled by possible ultraslow variation of the solar constant and the tectonic state of the Earth; $a_{0,1,2}$, $b_{1,2,3,4}$, and $c_{0,2}$ are "rate constants" assumed to be positive; and $M(t)$ is external (e.g., Milankovitch) forcing taken to be the July insolation at 65°N normalized to zero mean and unit variance. In this formulation we have neglected any explicit external forcing of μ or N. Discussion of the qualitative physical basis of the system (1)–(3) is given by *Saltzman and Maasch* [1988].

To further reduce the system to a simpler form that is easier both to analyze and integrate numerically, we rescale (1)–(3) with the following transformations: $t = [a_0^{-1}]t^*$, $I' = [c_2/c_0(a_0/b_4)^{1/2}]X$, $\mu' = [c_2(a_1c_0)^{-1}(a_0/b_4)^{1/2}]Y$, and $N' = [(a_0/b_4)^{1/2}]Z$. Our system becomes

$$\dot{X} = -X - Y - uM(t^*) \tag{4}$$

$$\dot{Y} = -pZ + rY + sZ^2 - Z^2Y \tag{5}$$

$$\dot{Z} = -q(X + Z) \tag{6}$$

where $(\dot{}) = d(\ )/dt^*$, $p = a_1c_0b_2/a_0^2c_2$, $q = c_2/a_0$, $r = b_1/a_0$, $s = a_1b_3c_0(a_0^3b_4)^{-1/2}/c_2$, and $u = a_2c_0(b_4/a_0^3)^{1/2}/c_2$. From physical considerations we choose the time constant for the ice sheets, a_0^{-1}, to be 10 kyr and require that the slow response time of the deep ocean, c_2^{-1}, be no more than this value (i.e., $q > 1$).

In the above referenced previous work we showed that with no external forcing ($M = 0$) we could assign a set of values to the rate constants in (1)–(3) (including reasonable values of the time constants a_0^{-1} and c_2^{-1}) that give a credible account of the main ~100-kyr variations of I and μ as participants in a "natural oscillator" involving the third slow variable, N. Specifically, if we choose as reference parameter values $p = 1.0$, $q = 1.2$, $r = 0.8$, and $s = 0.8$, we obtain the oscillatory solution of period 100 kyr, shown in

Paper number 89JD02749.
0148-0227/90/89JD-02479$05.00

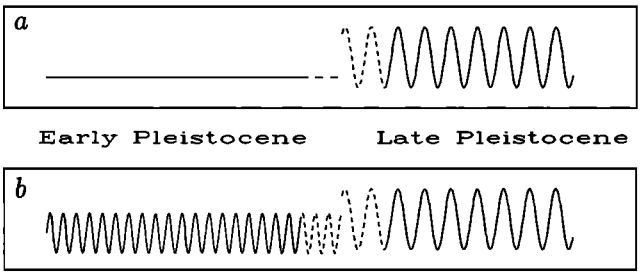

Fig. 1. Schematic illustration of two possible scenarios by which the free solutions of a model could account for the early and late Pleistocene.

Figure 2. Note that although information concerning phase and higher-frequency oscillations is missing from this unforced solution, the variations of model ice mass and CO_2 and their relative phases are in qualitative agreement with the observations. We note also that the limit cycle representing our solution takes place about a single unstable equilibrium, at $(X, Y, Z) = (0, 0, 0)$ where the eigenvalues are -1.79, $0.19 \pm 0.31i$).

A Forced Solution for the Late Pleistocene

With the addition of Earth orbital (Milankovitch) forcing we can also account for a good deal of the ~20- and ~40-kyr-period variance in the observations. The forcing also supplies the missing time phase information, i.e., the "pacemaker" [*Hays et al.*, 1976] properties of the forcing. In earlier attempts that we made to add Milankovitch forcing to previous models [*Saltzman et al.*, 1984; *Saltzman* 1987, 1988] we postulated a forcing function that was a linear combination of the variations in precessional index, obliquity, and eccentricity. Based on our sensitivity studies we thought that at least a small amount of eccentricity forcing was necessary to obtain a phase-locked solution (that is, a model solution showing rapid deglaciations at the times when they appear in the $\delta^{18}O$ record) for the last 500 kyr. Here we will demonstrate that it is possible to obtain a satisfactory solution over the last 500 kyr while forcing the system simply with the July insolation curve at 65°N.

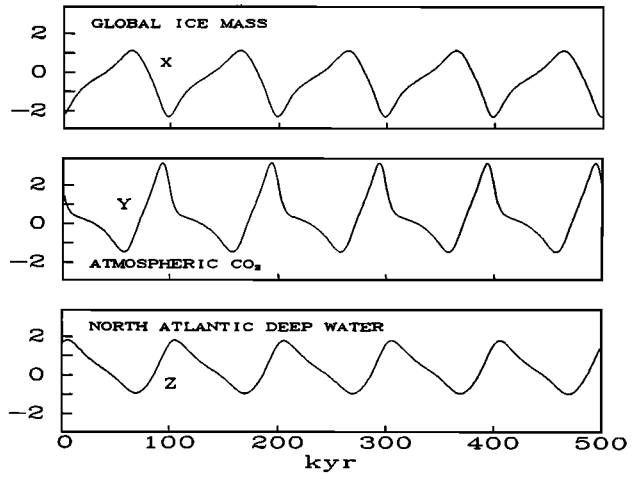

Fig. 2. Time-dependent periodic solution for (4)–(6) for an arbitrary 500 kyr period using parameter values $p = 1.0$, $q = 1.2$, $r = 0.8$, $s = 0.8$, and $u = 0.0$ (no forcing). (Top) X, representing global ice mass. (Middle) Y, representing atmospheric carbon dioxide (Bottom) Z, representing North Atlantic Deep Water.

The solutions of (4)–(6) using the reference values for p, q, r, and s but now setting $u = 0.7$ are presented in Figure 3 along with observational data for ice mass and atmospheric CO_2. This time-dependent solution was started from arbitrary initial conditions at 1 Ma. We see that there is a reasonably good agreement over the last 500 kyr between the model ice mass variations and the SPECMAP $\delta^{18}O$ curve [*Imbrie et al.*, 1984], and between model CO_2 variations and the CO_2 variations inferred from both the Vostok ice core [*Barnola et al.*, 1987] and the $\Delta\delta^{13}C$ record from core V19-30 [*Shackleton and Pisias*, 1985]. The timing of the last five terminations (denoted by the vertical dashed lines in Fig 3) are determined by a phase lock with the external forcing and appear to be about the same in the model as they are in the observed record. Also the relative phases between ice mass and CO_2 are in general agreement with the observations, as they were in the free solution [*Imbrie et al.*, 1990].

For comparison in the frequency domain we have made a spectral analysis of both the free and forced model solution for X (ice mass). The results are shown in Figure 4 along with the spectra for the forcing function and the SPECMAP curve. As is readily apparent, the forcing has little power at

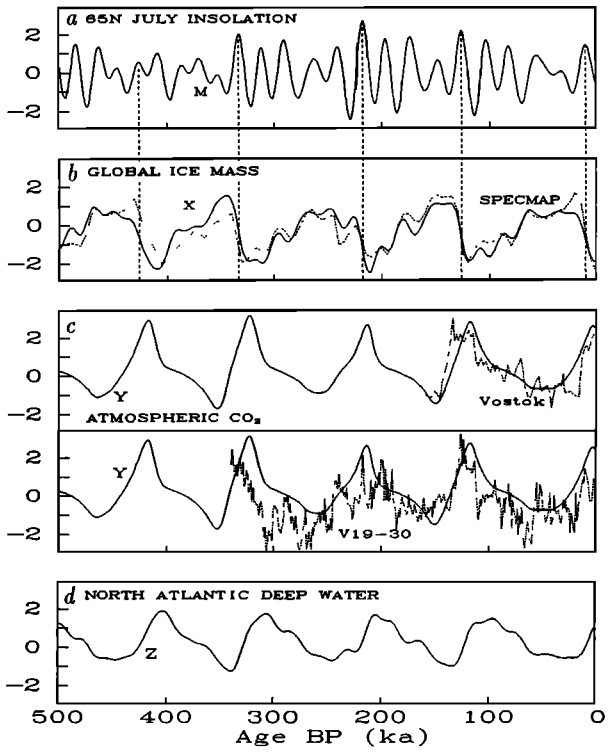

Fig. 3. Time-dependent forced solution for the last 500 kyr starting from arbitrary initial conditions at 1 Ma using the same p, q, r, and s values as in Figure 2, but now with $u = 0.7$. (*a*) Normalized July insolation curve at 65°N, M, that was used to force the model. (*b*) Comparison of forced solution for X (solid curve) with variations in global ice mass as inferred from the SPECMAP $\delta^{18}O$ curve (dashed curve). (*c*) Comparison of forced solution for Y (solid curves) with the predictions regarding CO_2 variations (dashed curves) implied by the recent Vostok ice core measurements [*Barnola et al.*, 1987] and the $\Delta\delta^{13}C$ record from equatorial Pacific core V19-30 [*Shackleton and Pisias*, 1985). (*d*) Forced solution for Z which is our model prediction for the time evolution of North Atlantic Deep Water. For the purpose of comparison all of the observed data (shown by dashed curves) have been normalized to have the same mean and variance as the model solution.

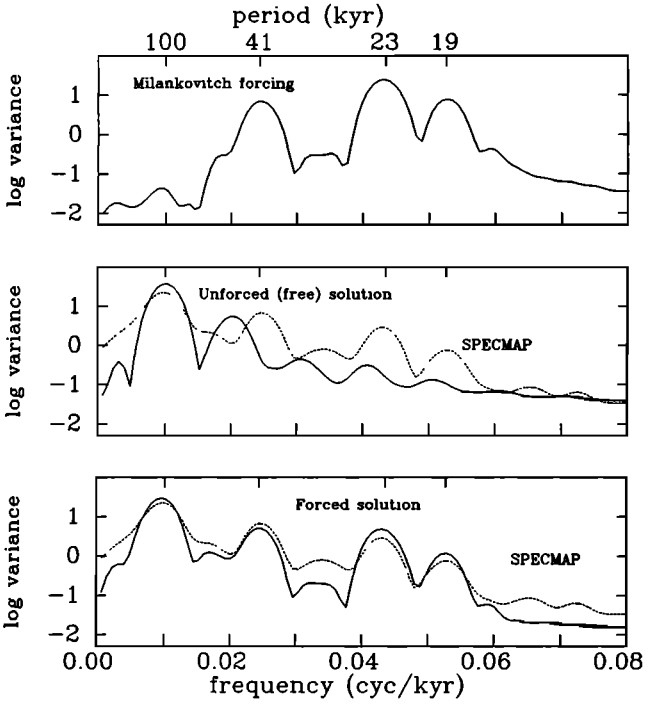

Fig. 4. (Top) Variance spectrum of the July insolation received at 65°N from 0–500 ka. (Middle) Variance spectrum of the unforced (free) solution for X shown in shown in upper panel of Figure 3 (solid curve), compared with the spectrum of our target curve shown in Figure 3*b* (dashed curve), both for 500 kyr records. (Bottom) Variance spectrum of the forced solution for X shown in Figure 3*b* (solid curve) again compared with the spectrum of the target curve (dashed curve), both for 500-kyr records.

periods near 100 kyr. In the model the 100-kyr period is the result of the free oscillation (reflected by the large peak seen in the spectra of both the free and forced solutions). There is excellent agreement between the model and the SPECMAP spectrum, but it must be recognized that the SPECMAP curve has been tuned to some extent to include the 41-, 23-, and 19-kyr periods that are present in M.

At this point we have a physically plausible model that yields solutions compatible with the observational evidence for the last 500 kyr. Our problem now is to determine whether the model is also capable of exhibiting a transition to this solution from an earlier state in which there are no 100-kyr oscillations, as discussed in the introduction. Such a transition is possible as an auto-bifurcation of a multiple equilibrium regime [*Saltzman and Sutera*, 1987] or, perhaps more likely, as a consequence of a progressive change in at least one of the parameters, which can be viewed as an externally forced "control" parameter [cf. *Oerlemans*, 1984; *Watts and Hayder*, 1983; *Ghil*, 1984; *Saltzman et al.*, 1984], leading to a bifurcation of the type illustrated in Figure 1. Since the general character of Milankovitch forcing varies only very slightly over the full Pleistocene [*Berger and Pestiaux*, 1984], some new, possibly tectonic, forcing might be involved. In the context of this scenario it would be this new forcing associated with the control parameter change that "turns on," i.e., "causes," the major 100-kyr-period ice age cycle in the late Pleistocene. One possibility is that some progressive ocean floor sill growth or erosion in the North Atlantic and Pacific can gradually modify the effect of ice on NADW production; another is that slow uplift of the Tibetan Plateau and western North America modified global airflow in a manner favoring cooler conditions in critical northern hemisphere locations [*Ruddiman et al.*, 1986], or modified weathering processes and hence the CO_2 concentration in the atmosphere [*Raymo et al.*, 1988]. In the following section we shall give a fuller discussion of the parameter range for which we can find the transition capability of our model, as well as further discussion of the possible role of forcing in accounting for more of the details of the full Pleistocene variations.

Bifurcation Properties of the Model

In order to now modify the model in accordance with the observational constraints imposed by the early-late Pleistocene transition we first need to explore in more detail the behavior of the system as a function of the model parameters. A change in the parameter values means not only a change in the dynamical behavior of the system, but also in the location and stability of the system's equilibrium points. It is possible that the nonstationarity of climate data, including jumps and trends in mean, variance, and periodicity, could be the result of transitions in phase space from the neighborhood of one equilibrium point to another due to a change in a key parameter of the model. To systematically explore this possibility for bifurcation, we shall begin by examining where the equilibrium points occur in phase space as a function of the model parameters. Then with the parameter values for which equilibrium points are real the linear stability properties will be determined. This involves calculation of the eigenvalues at each of these equilibrium points. With this information concerning the equilibrium points and their stability as a function of the model parameters we then know what to expect dynamically (i.e., steady state or possible limit cycle) and hence are able to choose a region in parameter space that can provide solutions having features compatible with the observations. Finally, we numerically integrate the system to obtain time dependent solutions of the system as a response to variations of the parameters that can give at least qualitative agreement with the observed record. We will show an example of a full Pleistocene free solution as well as one with external (Milankovitch) forcing.

Equilibrium Points

As is often the case when dealing with nonlinear dynamical systems, analytical solutions for the equilibrium points and their linearized stability (eigenvalues) can be difficult to derive. This is certainly true for the system governed by (4)–(6), and thus in order to learn how equilibrium points and stability vary as a function of changing a parameter of the model, we resort to numerical computation.

The equilibrium points (designated by a hat) for the unforced nondimensionalized system (4)–(6) are obtained by solving the following equations simultaneously:

$$-\hat{X}-\hat{Y}=0 \tag{7}$$

$$-p\hat{Z}+r\hat{Y}+s\hat{Z}^2-\hat{Z}^2\hat{Y}=0 \tag{8}$$

$$-q\hat{X}-q\hat{Z}=0 \tag{9}$$

Equations (7)–(9) may be reduced to a single cubic equation in terms of $\hat{X}$ of the form

$$\hat{X}^3 + s\hat{X}^2 + (p - r)\hat{X} = 0 \qquad (10)$$

One of the roots for (10) is the trivial solution $\hat{X}_0 = 0$, while the other two are

$$\hat{X}_{1,2} = \frac{-s \pm \sqrt{s^2 - 4(p - r)}}{2}$$

Note that by convention we have chosen to denote the equilibrium point $\hat{X} = 0$ with a subscript 0 while the other two equilibrium points are denoted by subscripts 1 and 2 and are ordered such that $\hat{X}_1 \geq \hat{X}_2$. The solutions of (10), along with substitution back into (7) and (9) to obtain the corresponding values for $\hat{Y}$ and $\hat{Z}$, give us the equilibrium points for any given set of model parameters ($\hat{Y} = \hat{Z} = -\hat{X}$). To check that numerical round-off is insignificant, we substitute our calculations for $\hat{X}$, $\hat{Y}$, and $\hat{Z}$ back into the original equations for $\dot{X}$, $\dot{Y}$, and $\dot{Z}$, finding that each are satisfied to at least $O(10^{-17})$.

Only real equilibrium points, such as always prevail for $\hat{X}_0$, have a physical meaning. However, it is easily seen that variations in p, r, or s can result in the movement of the other two equilibrium points onto or off of the real plane. If $s^2 - 4(p - r) \geq 0$, then $\hat{X}_1$ and $\hat{X}_2$ are real and hence could possibly represent either a new steady state solution or unstable points about which a new limit cycle solution might exist.

Stability

The dynamical behavior of the system near the above equilibrium points depends on the eigenvalues of the stability matrix for the system evaluated at these equilibrium points. The standard method used to obtain these eigenvalues may be summarized as follows:

First the system is linearized in the vicinity of the steady state. Then we find solutions for the linearized set of equations of the form $\vec{r}e^{\lambda t}$, where λ is the eigenvalue and $\vec{r}$ the corresponding eigenvector. In matrix form the problem we must solve is simply $(\mathbf{J} - \lambda\mathbf{I})\vec{r} = 0$, $\mathbf{J}$ being the Jacobian matrix and $\mathbf{I}$ the identity matrix. This can only be true for $\vec{r} \neq 0$ (i.e., nontrivial solutions) if $\det(\mathbf{J} - \lambda\mathbf{I}) = 0$, which for (4)–(6) means

$$\begin{vmatrix} (-1 - \lambda) & -1 & 0 \\ 0 & (r - \hat{Z}^2 - \lambda) & (-p + 2s\hat{Z} - 2\hat{Y}\hat{Z}) \\ q & 0 & (-q - \lambda) \end{vmatrix} = 0$$

The numerical solution of this determinant is then found using EISPACK subroutines [*Garbow et al.*, 1977]. As a check we then expand the determinant and use the fact that $\hat{Y} = \hat{Z} = -\hat{X}$ to obtain a cubic equation in λ of the form

$$\lambda^3 + [q - r + 1 + \hat{X}(\hat{X} - 1)]\lambda^2 + [q(1 - r + \hat{X}^2) - r]\lambda$$

$$+ q[p - r + (2s + 3\hat{X})\hat{X}] = 0$$

into which we can then substitute the eigenvalues found using EISPACK. The convention that we shall adopt for distinguishing each of the three eigenvalues at a given equilibrium point is to assign each a two-digit subscript such that λ_{ij} denotes the jth eigenvalue at the ith equilibrium point. Also by convention we have ordered the eigenvalues as follows: (1) If all three eigenvalues are real then $\lambda_{i1} \geq \lambda_{i2} \geq \lambda_{i3}$. (2) If only one eigenvalue is real and the other two form a complex conjugate pair, then λ_{i1} is the complex eigenvalue with the positive imaginary part, λ_{i2} is the complex eigenvalue with the negative imaginary part, and λ_{i3} is the real eigenvalue.

If all three eigenvalues have negative real parts, the equilibrium point is stable and will tend to be the attractor for a probability maximum, while if one or more of the eigenvalues have a positive real part the equilibrium point is unstable and will tend to coincide with a probability minimum. Both the stable and unstable equilibria can be further subdivided into those at which all three eigenvalues are real (exponentially stable or unstable) and those at which one eigenvalue is real and the other two are a complex conjugate pair (spirally stable or unstable).

Bifurcation Properties Near the Reference State

To illustrate the dependence of the equilibrium points and their stability on p, q, r, and s in the vicinity of the reference parameter values ($p = 1.0$, $r = 0.8$, $q = 1.2$, and $s = 0.8$) used to obtain the solutions shown in Figure 2, we will vary each parameter over a range of 0 to 2. Recall that for these reference parameters the system has only one real equilibrium point (0,0,0) which is spirally unstable. By allowing a

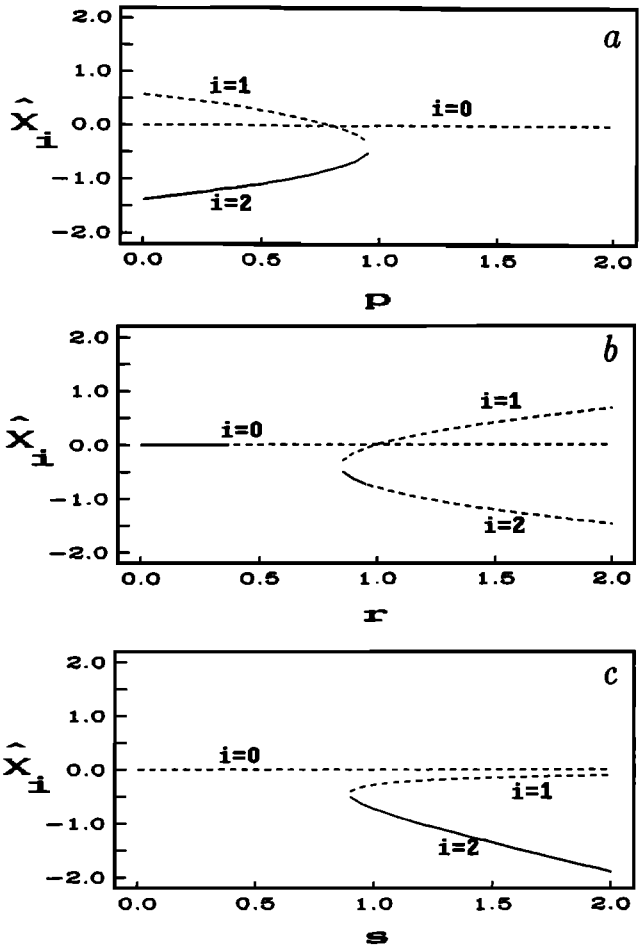

Fig. 5. Equilibrium points as a function of parameters. Dashed lines and solid lines indicate unstable and stable equilibrium points, respectively. (*a*) $\hat{X}_i$, $i = 0, 1, 2$ as a function of p while q, r, and s are held equal to reference values 1.2, 0.8, and 0.8 respectively. (*b*) Same as Figure 5*a* except now p is held constant at reference value 1.0 and r is allowed to vary. (*c*) Same as Figure 5*a* except now p is held constant at reference value 1.0 and s is allowed to vary.

single parameter to change while holding the others fixed at the reference values we can determine regions of parameter space where all three equilibrium points are real. As can be seen from (10), the equilibria are not a function of q. However, as we vary p, r, and s there is movement of equilibria onto and off of the real plane. The real equilibrium points holding all but one parameter constant are shown in Figure 5 with unstable points denoted by a dashed line and stable points by a solid line. The numerical values of the equilibrium points and their eigenvalues (when the equilibrium points are real) are given in Tables 1 – 4 as a function of p, q, r, and s, respectively.

The changes in the properties of the system in two dimensions of parameter space, p and r, are presented in Figure 6. These maps are intended to portray the stability of the system as a function of variations in both p and r while holding q and s at constant values. The key for the type of stability found in each of the regions numbered 1 through 6 may be summarized as follows: Regions of the parameter space where an equilibrium point is exponentially unstable (three real eigenvalues) are numbered 5 (two positive, one negative), or 4 (one positive, two negative). Regions where equilibrium points are exponentially stable (three negative real eigenvalues) are numbered 1. Regions of spirally stable equilibrium points (one eigenvalue is neagative real and two are complex with a negative real part) are numbered 2. Regions where equilibrium points are spirally unstable (one eigenvalue is negative real and two are complex with a positive real part) are numbered 3. Crossing from region 2 to region 3 represents a Hopf-type bifurcation. It is within

TABLE 1. Equilibrium Points and Their Eigenvalues as a Function of p With q, r, and s Held Equal to Reference Values 1.2, 0.8, and 0.8, Respectively

p	Eigenvalues at $\hat{X}_0$: $\lambda_{01}, \lambda_{02}, \lambda_{03}$	Equilibrium Points $\neq 0$: $\hat{X}_1, \hat{X}_2$	Eigenvalues at $\hat{X}_1$: $\lambda_{11}, \lambda_{12}, \lambda_{13}$	Eigenvalues at $\hat{X}_2$: $\lambda_{21}, \lambda_{22}, \lambda_{23}$
0.0	$0.80, -1.00, -1.20$	$0.58, -1.38$	$0.13 \pm 0.82i, -1.99$	$-0.48 \pm 1.07i, -2.35$
0.1	$0.77, -0.81, -1.36$	$0.53, -1.33$	$0.14 \pm 0.76i, -1.96$	$-0.44 \pm 1.05i, -2.28$
0.2	$0.73, -0.69, -1.44$	$0.47, -1.27$	$0.15 \pm 0.70i, -1.93$	$-0.41 \pm 1.02i, -2.21$
0.3	$0.69, -0.58, -1.51$	$0.41, -1.21$	$0.16 \pm 0.63i, -1.89$	$-0.37 \pm 0.99i, -2.14$
0.4	$0.64, -0.48, -1.56$	$0.35, -1.15$	$0.17 \pm 0.56i, -1.86$	$-0.33 \pm 0.94i, -2.07$
0.5	$0.59, -0.38, -1.61$	$0.28, -1.08$	$0.18 \pm 0.47i, -1.83$	$-0.28 \pm 0.89i, -2.00$
0.6	$0.53, -0.28, -1.65$	$0.20, -1.00$	$0.18 \pm 0.36i, -1.79$	$-0.23 \pm 0.83i, -1.94$
0.7	$0.45, -0.16, -1.69$	$0.11, -0.91$	$0.17 \pm 0.22i, -1.76$	$-0.18 \pm 0.75i, -1.87$
0.8	$0.33, 0.00, -1.73$	$0.00, -0.80$	$0.33, 0.00, -1.73$	$-0.12 \pm 0.64i, -1.81$
0.9	$0.18 \pm 0.19i, -1.76$	$-0.16, -0.65$	$0.40, -0.13, -1.69$	$-0.04 \pm 0.47i, -1.74$
1.0	$0.19 \pm 0.31i, -1.79$	$-0.40 \pm 0.20i$		
1.1	$0.21 \pm 0.39i, -1.82$	$-0.40 \pm 0.37i$		
1.2	$0.22 \pm 0.46i, -1.85$	$-0.40 \pm 0.49i$		
1.3	$0.24 \pm 0.52i, -1.87$	$-0.40 \pm 0.58i$		
1.4	$0.25 \pm 0.56i, -1.90$	$-0.40 \pm 0.66i$		
1.5	$0.26 \pm 0.61i, -1.92$	$-0.40 \pm 0.74i$		
1.6	$0.27 \pm 0.65i, -1.94$	$-0.40 \pm 0.80i$		
1.7	$0.28 \pm 0.69i, -1.97$	$-0.40 \pm 0.86i$		
1.8	$0.29 \pm 0.72i, -1.99$	$-0.40 \pm 0.92i$		
1.9	$0.30 \pm 0.75i, -2.01$	$-0.40 \pm 0.97i$		
2.0	$0.31 \pm 0.78i, -2.03$	$-0.40 \pm 1.02i$		

TABLE 2. Equilibrium Points and Their Eigenvalues as a Function of q With p, r, and s Held Equal to Reference Values 1.0, 0.8, and 0.8, Respectively

q	Eigenvalues at $\hat{X}_0$: $\lambda_{01}, \lambda_{02}, \lambda_{03}$	Equilibrium Points $\neq 0$: $\hat{X}_1, \hat{X}_2$	Eigenvalues at $\hat{X}_1$: $\lambda_{11}, \lambda_{12}, \lambda_{13}$	Eigenvalues at $\hat{X}_2$: $\lambda_{21}, \lambda_{22}, \lambda_{23}$
0.0	$0.80, 0.00, -1.00$	$-0.40 \pm 0.20i$		
0.1	$0.73, 0.03, -1.06$	$-0.40 \pm 0.20i$		
0.2	$0.66, 0.05, -1.11$	$-0.40 \pm 0.20i$		
0.3	$0.59, 0.09, -1.17$	$-0.40 \pm 0.20i$		
0.4	$0.51, 0.13, -1.24$	$-0.40 \pm 0.20i$		
0.5	$0.41, 0.19, -1.30$	$-0.40 \pm 0.20i$		
0.6	$0.28 \pm 0.09i, -1.36$	$-0.40 \pm 0.20i$		
0.7	$0.27 \pm 0.17i, -1.43$	$-0.40 \pm 0.20i$		
0.8	$0.25 \pm 0.21i, -1.50$	$-0.40 \pm 0.20i$		
0.9	$0.23 \pm 0.25i, -1.57$	$-0.40 \pm 0.20i$		
1.0	$0.22 \pm 0.27i, -1.64$	$-0.40 \pm 0.20i$		
1.1	$0.21 \pm 0.29i, -1.71$	$-0.40 \pm 0.20i$		
1.2	$0.19 \pm 0.31i, -1.79$	$-0.40 \pm 0.20i$		
1.3	$0.18 \pm 0.33i, -1.86$	$-0.40 \pm 0.20i$		
1.4	$0.17 \pm 0.34i, -1.94$	$-0.40 \pm 0.20i$		
1.5	$0.16 \pm 0.35i, -2.02$	$-0.40 \pm 0.20i$		
1.6	$0.15 \pm 0.36i, -2.10$	$-0.40 \pm 0.20i$		
1.7	$0.14 \pm 0.37i, -2.18$	$-0.40 \pm 0.20i$		
1.8	$0.13 \pm 0.38i, -2.27$	$-0.40 \pm 0.20i$		
1.9	$0.12 \pm 0.38i, -2.35$	$-0.40 \pm 0.20i$		
2.0	$0.12 \pm 0.39i, -2.43$	$-0.40 \pm 0.20i$		

TABLE 3. Equilibrium Points and Their Eigenvalues as a Function of r With p, q, and s Held Equal to Reference Values 1.0, 1.2, and 0.8, Respectively

r	Eigenvalues at $\hat{X}_0$: $\lambda_{01}, \lambda_{02}, \lambda_{03}$	Equilibrium Points $\neq 0$: $\hat{X}_1, \hat{X}_2$	Eigenvalues at $\hat{X}_1$: $\lambda_{11}, \lambda_{12}, \lambda_{13}$	Eigenvalues at $\hat{X}_2$: $\lambda_{21}, \lambda_{22}, \lambda_{23}$
0.0	$-0.15 \pm 0.78i, -1.90$			
0.1	$-0.11 \pm 0.75i, -1.88$			
0.2	$-0.07 \pm 0.71i, -1.87$			
0.3	$-0.02 \pm 0.67i, -1.85$			
0.4	$0.02 \pm 0.63i, -1.84$			
0.5	$0.06 \pm 0.57i, -1.83$			
0.6	$0.11 \pm 0.50i, -1.81$			
0.7	$0.15 \pm 0.42i, -1.80$			
0.8	$0.19 \pm 0.31i, -1.79$			
0.9	$0.24 \pm 0.10i, -1.78$	$-0.16, -0.65$	$0.50, -0.11, -1.72$	$0.02 \pm 0.46i, -1.761$
1.0	$0.57, 0.00, -1.77$	$0.00, -0.80$	$0.57, 0.00, -1.77$	$0.00 \pm 0.65i, -1.845$
1.1	$0.75, -0.09, -1.76$	$0.11, -0.91$	$0.57, 0.13, -1.81$	$-0.01 \pm 0.76i, -1.917$
1.2	$0.90, -0.15, -1.75$	$0.20, -1.00$	$0.51, 0.31, -1.85$	$-0.01 \pm 0.85i, -1.983$
1.3	$1.04, -0.20, -1.74$	$0.28, -1.08$	$0.46 \pm 0.18i, -1.89$	$-0.01 \pm 0.93i, -2.044$
1.4	$1.17, -0.24, -1.73$	$0.35, -1.15$	$0.50 \pm 0.27i, -1.93$	$-0.01 \pm 0.99i, -2.100$
1.5	$1.29, -0.27, -1.72$	$0.41, -1.21$	$0.55 \pm 0.34i, -1.96$	$-0.01 \pm 1.05i, -2.153$
1.6	$1.41, -0.30, -1.71$	$0.47, -1.27$	$0.58 \pm 0.39i, -1.99$	$-0.01 \pm 1.10i, -2.203$
1.7	$1.53, -0.32, -1.70$	$0.53, -1.33$	$0.62 \pm 0.44i, -2.02$	$-0.01 \pm 1.15i, -2.251$
1.8	$1.64, -0.35, -1.69$	$0.58, -1.38$	$0.66 \pm 0.49i, -2.05$	$-0.00 \pm 1.19i, -2.297$
1.9	$1.75, -0.37, -1.69$	$0.63, -1.43$	$0.69 \pm 0.53i, -2.07$	$-0.00 \pm 1.23i, -2.341$
2.0	$1.86, -0.38, -1.68$	$0.68, -1.48$	$0.72 \pm 0.56i, -2.10$	$0.00 \pm 1.27i, -2.383$

TABLE 4. Equilibrium Points and Their Eigenvalues as a Function of s With p, q, and r Held Equal to Reference Values 1.0, 1.2, and 0.8, Respectively

s	Eigenvalues at $\hat{X}_0$: $\lambda_{01}, \lambda_{02}, \lambda_{03}$	Equilibrium Points $\neq 0$: $\hat{X}_1, \hat{X}_2$	Eigenvalues at $\hat{X}_1$: $\lambda_{11}, \lambda_{12}, \lambda_{13}$	Eigenvalues at $\hat{X}_2$: $\lambda_{21}, \lambda_{22}, \lambda_{23}$
0.0	$0.19 \pm 0.31, -1.79$			
0.1	$0.19 \pm 0.31, -1.79$			
0.2	$0.19 \pm 0.31, -1.79$			
0.3	$0.19 \pm 0.31, -1.79$			
0.4	$0.19 \pm 0.31, -1.79$			
0.5	$0.19 \pm 0.31, -1.79$			
0.6	$0.19 \pm 0.31, -1.79$			
0.7	$0.19 \pm 0.31, -1.79$			
0.8	$0.19 \pm 0.31, -1.79$			
0.9	$0.19 \pm 0.31, -1.79$	$-0.40, -0.50$	$0.23, -0.12, -1.67$	$-0.500.01 \pm 0.19, -1.68$
1.0	$0.19 \pm 0.31, -1.79$	$-0.28, -0.72$	$0.40, -0.22, -1.66$	$-0.72 - 0.11 \pm 0.46, -1.71$
1.1	$0.19 \pm 0.31, -1.79$	$-0.23, -0.87$	$0.44, -0.24, -1.66$	$-0.87 - 0.21 \pm 0.58, -1.74$
1.2	$0.19 \pm 0.31, -1.79$	$-0.20, -1.00$	$0.47, -0.25, -1.66$	$-1.00 - 0.31 \pm 0.67, -1.78$
1.3	$0.19 \pm 0.31, -1.79$	$-0.18, -1.12$	$0.48, -0.26, -1.65$	$-1.12 - 0.41 \pm 0.72, -1.83$
1.4	$0.19 \pm 0.31, -1.79$	$-0.16, -1.24$	$0.49, -0.26, -1.65$	$-1.24 - 0.52 \pm 0.76, -1.89$
1.5	$0.19 \pm 0.31, -1.79$	$-0.15, -1.35$	$0.49, -0.26, -1.65$	$-1.35 - 0.63 \pm 0.77, -1.98$
1.6	$0.19 \pm 0.31, -1.79$	$-0.14, -1.46$	$0.50, -0.26, -1.65$	$-1.46 - 0.73 \pm 0.77, -2.09$
1.7	$0.19 \pm 0.31, -1.79$	$-0.13, -1.57$	$0.50, -0.27, -1.65$	$-1.57 - 0.82 \pm 0.74, -2.24$
1.8	$0.19 \pm 0.31, -1.79$	$-0.12, -1.68$	$0.51, -0.27, -1.65$	$-1.68 - 0.90 \pm 0.70, -2.43$
1.9	$0.19 \pm 0.31, -1.79$	$-0.11, -1.79$	$0.51, -0.27, -1.65$	$-1.79 - 0.96 \pm 0.65, -2.69$
2.0	$0.19 \pm 0.31, -1.79$	$-0.11, -1.89$	$0.51, -0.27, -1.65$	$-1.89 - 1.00 \pm 0.60, -2.99$

the parameter ranges denoted by regions 3, 4, and 5 where we can expect a stable limit cycle.

Note from Figure 6 that for our reference parameters (denoted by the dot) there exists only one real equilibrium point (region 3) and that the stability at this point is spiral unstable. We also note that an important consequence of adding asymmetry to the model ($s > 0$) is that the upper equilibrium point ($\hat{X}_1$) can be unstable while the lower one ($\hat{X}_2$) is stable. This differs from symmetric cases where $\hat{X}_1$ and $\hat{X}_2$ are either both stable or both unstable.

AN EXTENDED SOLUTION FOR THE FULL PLEISTOCENE

Using the information gained in the preceding section, we are now in a position to explore what kinds of variability can be explained by free solutions of the model (no external forcing). As is shown in the following example, the transition in the mean, variance, and the appearance of a ~100-kyr cycle as well as a phase relationship between ice mass and CO_2 can all be at least qualitatively modeled in the spirit of the scenario portrayed in Figure 1*a*. Here the phase of the free solutions is not only a function of initial conditions, as it was for the unforced late Pleistocene example shown in Figure 2, but also depends on variations of model parameters. Since the actual timing of deglaciations may also be determined by external orbital forcing (examples to follow) we need not be concerned at this point with comparing free solutions with the observed data in more than a qualitative sense.

The transition from a solution which is influenced by a stable equilibrium point to one influenced by an unstable point can be accomplished by increasing p and r such that

KEY

Code	λ_{i1}	λ_{i2}	λ_{i3}
1	real < 0	real < 0	real < 0
2	re(cmplx) < 0	re(cmplx) < 0	real < 0
3	re(cmplx) > 0	re(cmplx) > 0	real < 0
4	real > 0	real < 0	real < 0
5	real > 0	real > 0	real < 0
6	re(cmplx) < 0	re(cmplx) < 0	real > 0
7	Complex Equilibrium Point		

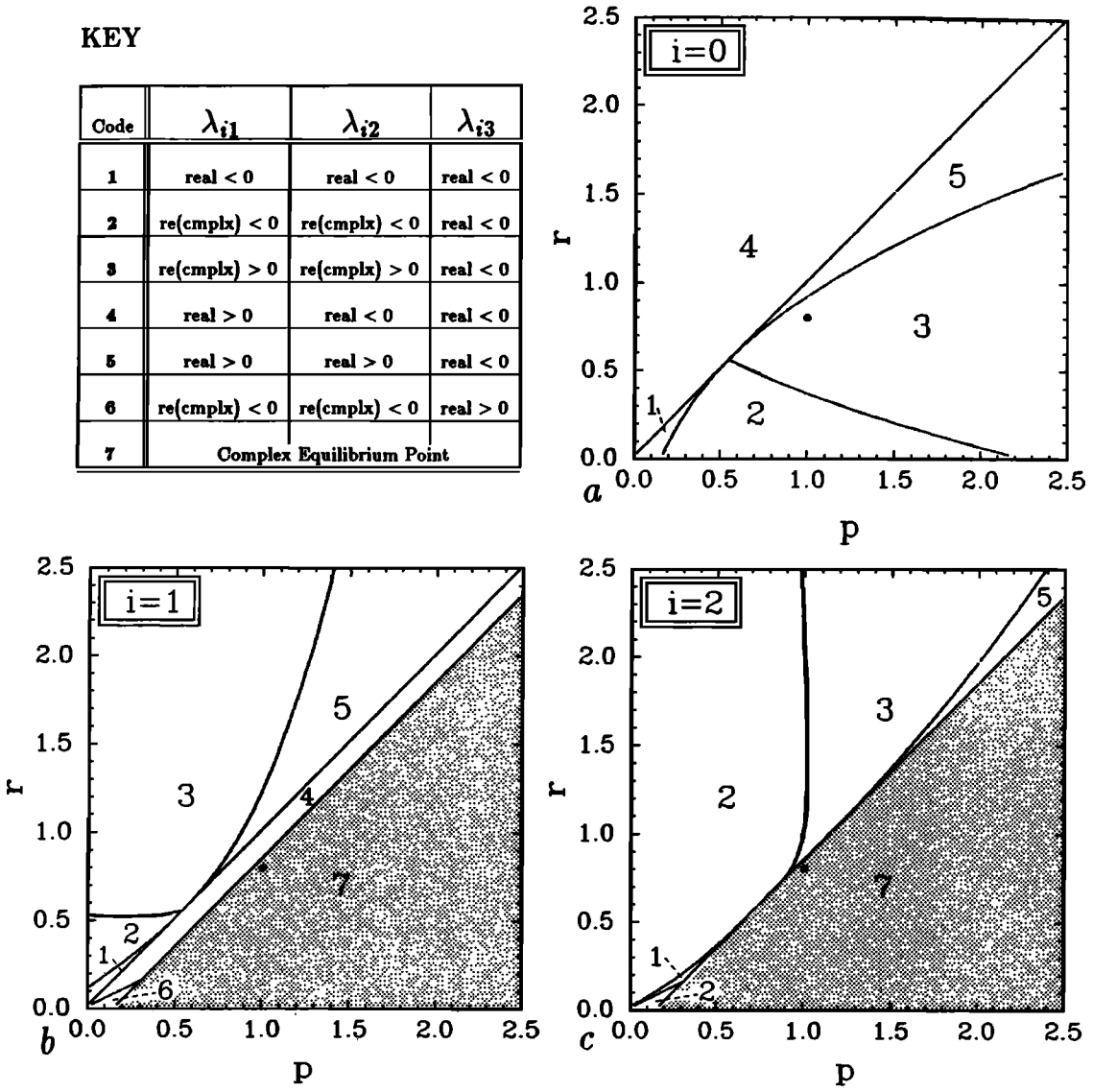

Fig. 6. Stability of equilibrium points (a) $\hat{X}_0$, (b) $\hat{X}_1$, and (c) $\hat{X}_2$ as a function of varying both p and r while holding q and s equal to reference values 1.2 and 0.8, respectively. The dot indicates location of "reference" parameters.

in the parameter space shown in Figure 6, the lower equilibrium point ($i = 2$) moves from region 2 to the "reference" equilibrium point (which we have shown is capable of simulating the late Pleistocene). To illustrate this possibility, in Figure 7 we show an example in which we have integrated the system for 2 million years starting from arbitrary intial conditions with the parameter values $q = 1.2$ and $s = 0.8$, but allowing p and r to increase linearly through the bifurcation point $(p, r) = (0.92, 0.76)$ from $0.8 \rightarrow 1.0$ and $0.7 \rightarrow 0.8$, respectively. Although choosing to vary p and r in this manner is clearly arbitrary, we argue that our earlier assumption that each of the model coefficients is a positive "constant" is also arbitrary and should be expected to break down over a period of time as long as millions of years. Recall that these coefficients represent not only a multitude of fast physical processes that we believe cannot be explicitly parameterized (thus leading us to our inverse modeling approach), but also represent absolute equilibrium values that are likely to be connected to longer-term tectonic forcing. It may in fact be possible to partially constrain the bounds over which the model parameters can vary (and in principle they are probably all functions of time) by using available information on very long term trends (~ millions of years) in the mean of global ice mass and atmospheric CO_2. However, for the time being we shall vary only p and r in a linear fashion in order to illustrate the model's capability of accounting for the

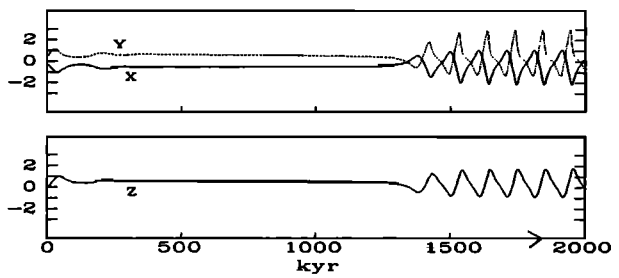

Fig. 7. Unforced (free) solution for (4)–(6) with $q = 1.2$, $s = 0.8$, and p and r varying linearly between $0.8 \rightarrow 1.0$ and $0.7 \rightarrow 0.8$, respectively. (Top) Model solutions for X (solid) and Y (dashed). (Bottom) Model solution for Z.

mid-Pleistocene transition and leave the longer-term (i.e., Cenozoic) problem for a future study. The solution shown in Figure 7 illustrates how slow linear changes in control parameters, representing the effects of slow tectonic changes, can lead to an abrupt change in the climatic response when a critical value is reached.

As done previously, we next force the system with the July insolation received at 65°N over the full Pleistocene. We again choose the values $q = 1.2$ and $s = 0.8$, and we allow p and r to increase linearly from $0.8 \rightarrow 1.0$ and $0.7 \rightarrow 0.8$ respectively, achieving the critical bifurcation values of p and r at $\sim$ 900 ka, but now we also set $u = 0.7$. The results of integrating the system with orbital forcing, shown in Figure 8, is capable of reproducing not only the emergence of the 100-kyr cycle in the late Pleistocene, but now also the shorter-period oscillations believed to be connected with changes in obliquity and precession. Also, in contrast to the free solution shown in Figure 7, the phase of the global ice mass is locked by the forcing so that major terminations in the late Pleistocene occur at the time at which they appear to occur in the $\delta^{18}O$ record. Spectral analysis of the early (1800 – 1000 ka) and late (800 – 0 ka) portions of the model solution for ice mass is shown in Figure 9.

SUMMARY AND CONCLUSIONS

In an attempt to account for the observed chronology of the full 2-million-year Pleistocene climatic record, a previously formulated dynamical model of of the late Pleistocene ice ages is extended to include (1) additive Earth orbital forcing (summer insolation changes at 65°N) and (2) tectonic forcing in the form of a postulated variation in the multiplicative parameters (rate constants) of the model system. This model is based on the hypothesis that the global CO_2 system can provide the instability to drive a natural oscillation involving feedbacks between the cryosphere, atmosphere, and ocean. While many of the main features exhibited by observed records of global ice mass and carbon dioxide in the late Pleistocene can be deduced as such a free oscillation, with the addition of the external Earth orbital forcing the model can account for a significant amount of the remaining observed variance and covariance of these climatic variables over the last 500 kyr including shorter-period oscillations (i.e., ~40 and ~20 kyr) and also can provide the temporal phase information (i.e., rapid deglaciations occurring at times consistent with the terminations as they appear in the $\delta^{18}O$ record).

To further investigate the possibility of modeling the mid-Pleistocene transition as the result of a bifurcation of the system, a complete structural analysis is made, including the determination of equilibria and stability as a function of model parameters. We assume that a slow, progressive change in model parameters associated with an as yet unidentified change in the tectonically forced equilibria of the system could be the cause of the mid-Pleistocene transition. Time-dependent solutions of the unforced system as a response to variations in two parameters are shown to be able to give at least qualitative agreement with the observed record. We again apply orbital forcing obtaining a solution for the full Pleistocene (including the mid-Pleistocene transition) that seems to include all of the features constituting what we believe is a minimally acceptable description of the observations.

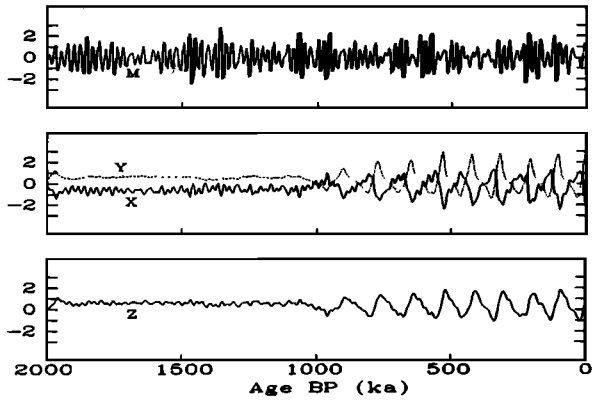

Fig. 8. Forced solution for (4)–(6) with $q = 1.2$, $s = 0.8$, $u = 0.7$, and p and r varying linearly between $0.8 \rightarrow 1.0$ and $0.7 \rightarrow 0.8$, respectively. (Top) Normalized 65°N July insolation curve (M) used as forcing. (Middle) Model solutions for X (solid) and Y (dashed). (Bottom) Model solution for Z.

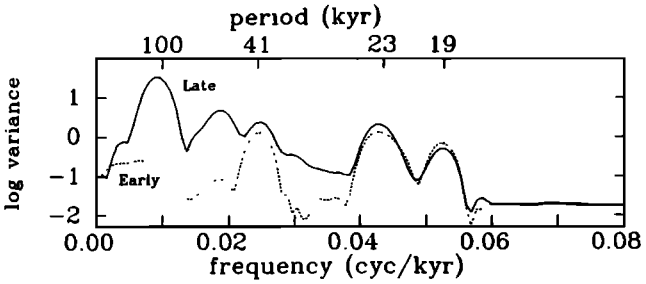

Fig. 9. Variance spectrum of the forced solution for X shown in Figure 8. The solid curve is the spectrum for the late Pleistocene (800–0 ka) portion of the record, and the dashed curve is spectrum for the early Pleistocene (1800–1000 ka).

Acknowledgments. This research has been supported by the Division of Atmospheric Sciences, National Science Foundation, under grant ATM-8802630 and by NASA under grant NAG8-785. We are grateful to John Imbrie and William Ruddiman for constructive reviews.

REFERENCES

Barnola, J. M., D. Raynaud, Y. S. Korotkevich, and C. Lorius, Vostok ice core provides 160,000-year record of atmospheric CO_2, *Nature, 329*, 408–414, 1987.

Berger, A., and P. Pestiaux, Accuracy and stability of the Quaternary terrestrial insolation, in *Milankovitch and Climate*, part I, edited by A. Berger, J. Imbrie, J. Hays, G. Kukla, and B. Saltzman, pp. 83–111, D. Reidel, Hingham, Mass., 1984.

Garbow, B., J. Boyle, J. Dongarra, and C. Molar, *Matrix Eigensystem Routines - EISPACK Guide Extension, Lect. Notes Comput. Sci.*, vol. 51, pp. 343, Springer-Verlag, New York, 1977.

Ghil, M., Climate sensitivity, energy balance models and oscillatory climate models, *J. Geophys. Res., 89*, 1280–1284, 1984.

Hays, J. D., J. Imbrie, and N. J. Shackleton, Variations in the Earth's orbit: Pacemaker of the ice ages, *Science, 194*, 1121–1132, 1976.

Imbrie, J., N. J. Shackleton, N. G. Pisias, J. J. Morley W. L. Prell, D. G. Martinson, J. D. Hays, A. McIntyre, and A. C. Mix, The orbital theory of Pleistocene climate: Support from a revised chronology of the marine $\delta^{18}O$ record, in *Milankovitch and Climate*, part I, edited by A. Berger, J. Imbrie, J. Hays, G. Kukla, and B. Saltzman, pp. 269–305, D. Reidel, Hingham, Mass., 1984.

Imbrie, J., A. McIntyre, and A. C. Mix, Oceanic response to orbital forcing in the late Quaternary: Observational and ex-

permintal strategies, in *Climate and Geoscience*, edited by J. C. Duplessy, A. Berger, and S. H. Schneider, Reidel, Hingham, Mass., in press, 1990.

Maasch, K. A., Statistical detection of the mid-Pleistocene transition, *Clim. Dyn.*, *2*, 133–143, 1988.

Oerlemans, J., On the origin of the ice ages, in *Milankovitch and Climate*, part II, edited by A. Berger, J. Imbrie, J. Hays, G. Kukla, and B. Saltzman, pp. 607–611, D. Reidel, Hingham, Mass., 1984.

Pisias, N. G. and T. C. Moore, The evolution of Pleistocene climate: A time series approach, *Earth and Planet. Sci. Lett.*, *52*, 450–458, 1981.

Raymo, M. E., W. F. Ruddiman, and P. N. Froelich, Influence of late Cenozoic mountain building on ocean geochemical cycles, *Geology*, *16*, 649–653, 1988.

Ruddiman, W. F., M. E. Raymo, and A. McIntyre, Matuyama 41,000-year cycles: North Atlantic Ocean and northern hemisphere ice sheets, *Earth Planet. Sci. Lett.*, *80*, 117–129, 1986.

Saltzman, B., Carbon dioxide and the $\delta^{18}O$ record of late Quaternary climatic change: A global model, *Clim. Dyn.*, *1*, 77–85, 1987.

Saltzman B., Modelling the slow climatic attractor, in *Physically-Based Modelling and Simulation of Climate and Climatic Change*: vol. 2, edited by M. E. Schlesinger, pp. 737–754, Kluwer, Dordrecht, 1988.

Saltzman, B., and K. A. Maasch, Carbon cycle instability as a cause of the late Pleistocene ice age oscillations: Modeling the asymmetric response, *Global Biogeochem. Cycles*, *2*, 177–185, 1988.

Saltzman, B., and A. Sutera, The mid-Quaternary climatic transition as the free response of a three-variable dynamical model, *J. Atmos. Sci.*, *44*, 236–241, 1987.

Saltzman B., A. R. Hansen, and K. A. Maasch, The late Quaternary glaciations as the response of a three-component feedback system to Earth-orbital forcing, *J. Atmos. Sci.*, *41*, 3380–3389, 1984.

Shackleton, N. J. and N. G. Pisias, Atmospheric carbon dioxide, orbital forcing, and climate, in *The Carbon Cycle and Atmospheric CO_2: Natural Variations Archean to Present, Geophys. Monogr. Ser.*, vol. 32, edited by E. T. Sundquist and W. S. Broecker, pp. 303–317, AGU, Washington, D.C., 1985.

Start G. G., and W. L. Prell, Evidence for two Pleistocene climatic modes: Data from DSDP site 502, in *New Perspectives in Climate Modelling*, edited by A. Berger and C. Nicolis, pp. 3–22, Elsevier, New York, 1984.

Watts, R. G. and M. E. Hayder, The origin of the 100-kiloyear ice sheet cycle, *J. Geophys. Res.*, *88*, 5163–5166, 1983.

K. A. Maasch and B. Saltzman, Department of Geology and Geophysics, P.O. Box 6666, Yale University, New Haven, CT 06511.

(Received April 5, 1989;
revised August 1, 1989;
accepted August 15, 1989)